

^{18}F -fluorothymidine kinetics of malignant brain tumors

Christiaan Schiepers · Wei Chen · Magnus Dahlbom ·
Timothy Cloughesy · Carl K. Hoh · Sung-Cheng Huang

Received: 1 September 2006 / Accepted: 3 December 2006
© Springer-Verlag 2007

Abstract

Purpose ^{18}F -labeled deoxy-fluorothymidine (FLT), a marker of cellular proliferation, has been used in PET tumor imaging. Here, the FLT kinetics of malignant brain tumors were investigated.

Methods Seven patients with high-grade tumors and two patients with metastases had 12 studies. After 1.5 MBq/kg ^{18}F -FLT had been administered intravenously, dynamic PET studies were acquired for 75 min. Images were reconstructed with iterative algorithms, and corrections applied for attenuation and scatter. Parametric images were generated with factor analysis, and vascular input and tumor output functions were derived. Compartmental models were used to estimate the rate constants.

Results The standard three-compartment model appeared appropriate to describe ^{18}F -FLT uptake. Corrections for blood volume, metabolites, and partial volume were necessary. Kinetic parameters were correlated with tumor pathology and clinical follow-up data. Two groups could be distinguished: lesions that were tumor predominant (TumP)

and lesions that were treatment change predominant (TrcP). Both groups had a widely varying k_1 (transport across the damaged BBB, range 0.02–0.2). Group TrcP had a relatively low k_3 (phosphorylation rate, range 0.017–0.027), whereas k_3 varied sevenfold in group TumP (range 0.015–0.11); the k_3 differences were significant ($p < 0.01$). The fraction of transported FLT that is phosphorylated [$k_3 / (k_2 + k_3)$] was able to separate the two groups ($p < 0.001$).

Conclusion A three-compartment model with blood volume, metabolite, and partial volume corrections could adequately describe ^{18}F -FLT kinetics in malignant brain tumors. Patients could be distinguished as having: (1) tumor-predominant or (2) treatment change-predominant lesions, with significantly different phosphorylation rates.

Keywords ^{18}F -FLT · Positron emission tomography · Brain tumor · Kinetic modeling · Factor analysis

Introduction

Imaging of glucose utilization rate is a routine diagnostic procedure in the work-up of cancer. Imaging cell proliferation has emerged as an avenue for characterizing and classifying neoplastic disease. Labeling of the antiviral drug 3'-deoxy-3'-fluorothymidine (FLT) with the positron emitter ^{18}F has provided a non-invasive way of studying the salvage pathway of DNA synthesis. FLT is phosphorylated by thymidine kinase-1 (TK1) and trapped inside the cell. Phosphorylated FLT appears resistant to degradation and is suitable for imaging with PET [1, 2]. The application of FLT phosphorylation as a marker of cell proliferation is based on the assumption that cellular FLT trapping is a representation of thymidine incorporation into DNA. This has been demonstrated in various tumor models, including

C. Schiepers (✉) · W. Chen · M. Dahlbom · S.-C. Huang
Department of Molecular and Medical Pharmacology,
David Geffen School of Medicine, University of California,
AR-144 CHS 10833 Le Conte Avenue,
Los Angeles, CA 90095-6942, USA
e-mail: cschiepers@mednet.ucla.edu

T. Cloughesy
Department of Neurology,
David Geffen School of Medicine,
University of California,
Los Angeles, CA, USA

C. K. Hoh
Department of Radiology, School of Medicine,
University of California,
San Diego, CA, USA

two glioma cell lines [3]. The ATP level is very important for the phosphorylation of FLT. ATP initiates a transition from a dimer to a tetramer structure of TK, which is about 20-fold more effective regarding the phosphorylation of FLT. Therefore, FLT can reflect cell proliferation, if there are no major differences in ATP levels. FLT can be used as a DNA chain terminator, but the incorporation of FLT into DNA is low, as has been demonstrated [4].

The clinical application of ^{18}F -labeled FLT in brain gliomas has been reported by Chen et al. [5]. In their study, the radiopharmaceuticals FDG and FLT were compared, and the uptake ratio of tumor to normal tissue in patients with brain gliomas was higher for FLT and the maximum uptake was reached earlier (5–10 min after injection) than for FDG. For high-grade gliomas, Chen et al. showed that FLT is a surrogate marker of cell proliferation and superior to FDG as a prognostic marker for patient survival.

FLT has also been used in lung cancer [6], colorectal cancer [7], and laryngeal cancer [8]. Visvikis et al. performed kinetic modeling of FLT in colorectal cancer [9] and Muzi et al., of FLT in lung cancer [10]. These studies revealed that metabolites play an important role. After intracellular phosphorylation, FLT is not further metabolized. The situation is entirely different in the vascular space. The liver metabolizes FLT to FLT-glucuronide in up to 40%, but the metabolite, fortunately, stays within the vascular pool. Muzi et al. also studied the mathematical aspects of the FLT model, and the boundary conditions were adopted in our implementation of the FLT kinetic model [11].

In the current study, we investigated the kinetics of malignant brain tumors in detail, and applied compartmental modeling to estimate the rate constants. The tracer kinetics were studied with an image-derived input and output function, i.e., time-activity curve (TAC) of blood clearance and tumor accumulation, respectively. Metabolite and partial volume corrections were applied to estimate FLT transport across the blood-brain barrier (BBB) and FLT influx into malignant brain tumors.

Materials and methods

Patients

The study population consisted of nine patients, seven with primary brain tumors and two with brain metastases. There were five men and four women, with an average age of 48 years (range 24–65). The study was approved by the Institutional Review Board, and all patients signed an informed consent to participate in this imaging study. Two patients were newly diagnosed, five had a recurrence, and two had a brain metastasis from a somatic tumor.

Histopathology revealed glioblastoma multiforme ($n=5$), oligodendroglioma ($n=2$, grade 3), lung cancer metastasis ($n=1$), and melanoma metastasis ($n=1$). Three of these nine patients had a repeat study, yielding a total of 12 studies. Three patients had multiple tumor locations that could be evaluated (two had three and one had two tumors). Thus, there were 18 separate tumor TACs that could be analyzed (Table 1).

Radiopharmaceutical preparation

FLT was synthesized by a modification of a previously reported procedure [12]. A dose of 1.5 MBq/kg (0.04 mCi/kg) ^{18}F -labeled FLT was used. No-carrier-added ^{18}F -fluoride was produced by 11-MeV proton bombardment of 95% ^{18}O -enriched water via the $^{18}\text{O}(\text{p},\text{n})^{18}\text{F}$ nuclear reaction. This aqueous ^{18}F -fluoride ion ($\sim 18,500$ MBq) was treated with potassium carbonate and Kryptofix 2.2.2. (Aldrich Chemical Co.). Water was evaporated by azeotropic distillation with acetonitrile. The dried K^{18}F /Kryptofix residue was reacted with the precursor of FLT (5'-*O*-[4,4'-dimethoxytrityl]-2,3'-anhydrothymidine) and then hydrolyzed with dilute HCl. The crude ^{18}F -labeled product was purified by semipreparative high-performance liquid chromatography (HPLC) (Phenomenex Aqua column, 25 cm \times 1 cm; 10% ethanol in water; flow rate, 5.0 ml/min) to give chemically and radiochemically pure ^{18}F -FLT in 555–1,110 MBq (6–12% radiochemical yield, decay corrected) amounts per batch. The chemical radiochemical purities of the product isolated from the semi-HPLC system were confirmed by an analytic HPLC method (Phenomenex Luna C18 column, 25 cm \times 4.1 mm; 10% ethanol in water; flow rate, 2.0 ml/min; 287-nm ultraviolet and radioactivity detection; specific activity, ~ 74 Bq/mmol) and found to be $>99\%$. The product was made isotonic with sodium chloride and sterilized by passing through a 0.22- μm Millipore filter into a sterile multidose vial. The final product was sterile and pyrogen free.

Image acquisition

PET imaging was performed using an ECAT HR+ system (CTI/Siemens, Knoxville, TN). A transmission scan of 5 min duration was acquired first, in 2-D mode. Subsequently, FLT was administered intravenously and a dynamic acquisition started. The emission images were acquired in 3-D mode. Twenty-six frames were acquired of 12 \times 15, 2 \times 30, 2 \times 60, and 14 \times 300 s duration. The images were reconstructed with iterative techniques, MAP (maximum a posteriori maximization) [13] for the transmission scan and OSEM (ordered subset expectation maximization consisting of eight iterations with six subsets) [14] for the emission scan. Corrections for attenuation and scatter were applied.

A Gaussian kernel with 5 mm full-width at half-maximum (FWHM) was used as a postreconstruction smoothing filter. The intrinsic spatial resolution (FWHM) of the equipment is 4.5 mm in the center of the field of view. In the reconstructed images the spatial resolution was 6.8 mm. The final reconstructed volume set had a matrix size of 128×128 and consisted of 63 planes, resulting in a voxel size of 2.45×2.45×2.425 mm.

Processing

Factor analysis (FA) was performed on this volume of reconstructed images [15]. After rebinning of the data into larger voxels (to speed up processing), the algorithm generated TACs for each voxel. The zooming, summation of planes, and rebinning produced an isometric dataset with 4.9×4.9×4.9 mm³ voxels that was used for further processing. TACs were generated for all voxels within the head contour. Each TAC was represented as a vector in a multidimensional space, and FA was performed on the complete vector set for the patient. For our implementation, three factors and their corresponding parametric or factor images were generated, representing the vessels, tumor, and residuals. Thresholding of the factor image representing vascular structures, e.g., the transverse and cavernous sinuses, with a 50% threshold created a volume of interest

(VOI). With this VOI, an image-based blood TAC was generated from the reconstructed dynamic PET images. Similarly, a tumor curve was created using a 75% threshold on the tumor factor image. The blood and tumor TACs were used for kinetic modeling.

Compartmental model

The model used is similar to the standard compartmental model for FDG [16, 17]. A detailed version of the three-compartment model for FLT, based on known biochemistry, was published by Muzi et al. [11]. They studied the mathematical behavior of the parameters, and provided a range for optimization of these parameters. Briefly, the model assumes a transport step of FLT from the vascular to the tissue space. There is no partitioning in the vascular space, and plasma and whole blood activity concentrations are the same [11]. In the tissue space, there is an exchangeable compartment (with intact FLT) and a trapped compartment of phosphorylated FLT (mono-, di-, and triphosphate-FLT). FLT is transported between plasma and tissue by the same transporters as thymidine and is trapped in the tissue. FLT is metabolized by the liver to FLT-glucuronide, which is present only in the vascular space, i.e., it is not transported into the brain tissue compartment. Kinetic modeling was used to estimate the values of the

Table 1 Individual data of all patients with number of studies performed and tumors analyzed

Patient	Pathology	Tumor grade	Type	Group	Time DP	Outcome	Study	Tumor	k_1	k_2	k_3	k_4	V_b	K	
1	GBM	IV	New	TumP	0.5	1 ^a	1	1	0.063	0.106	0.033	0.011	0.051	0.015	
								2	0.080	0.116	0.041	0.003	0.105	0.021	
								3	0.194	0.167	0.106	0.009	0.185	0.076	
2	GBM	IV	Rec	TumP	51	2 ^a	1	1	0.058	0.072	0.059	0.020	0.090	0.026	
								2	0.041	0.051	0.015	0.018	0.097	0.009	
								3	0.075	0.122	0.051	0.017	0.086	0.022	
								2	1	0.066	0.170	0.091	0.021	0.063	0.023
									2	0.074	0.069	0.042	0.007	0.106	0.028
3	0.085	0.131	0.060	0.019	0.096	0.027									
3	GBM	IV	Rec	TumP	7	4 ^a	1	1	0.060	0.096	0.030	0.015	0.061	0.014	
								2	1	0.031	0.072	0.051	0.026	0.032	0.013
4	Oligodendr	III	New	TumP	1	Alive	1	1	0.029	0.112	0.057	0.025	0.072	0.010	
5	Oligodendr	III	Rec	TumP	5	Alive	1	1	0.042	0.142	0.086	0.024	0.037	0.016	
6	GBM	IV	Rec	TrcP	39	7 ^a	1	1	0.200	0.205	0.027	0.019	0.310	0.023	
7	GBM	IV	Rec	TrcP	4	5 ^a	1	1	0.111	0.131	0.017	0.012	0.122	0.013	
								2	1	0.080	0.104	0.018	0.015	0.094	0.012
8	Lung cancer	IV	Met	TrcP	7	Alive	1	1	0.025	0.069	0.021	0.012	0.052	0.006	
9	Melanoma	IV	Met	TrcP	10	7 ^a	1	1	0.067	0.109	0.017	0.011	0.060	0.009	

A total of 18 lesions and TACs were available for analysis

Time DP time from diagnosis to PET in months, *GBM* glioblastoma multiforme, *Oligodendr* oligodendroglioma, *New* newly diagnosed, *Rec* recurrent disease, *Met* metastasis, *TumP* tumor-predominant lesions, *TrcP* treatment change-predominant lesions, k_1 – k_4 , V_b estimates of the five fitted parameters, K influx rate constant

^aDeath in months after PET (*Alive* indicates >22 months after PET)

four rate constants (k_1 , k_2 , k_3 , k_4) from each tumor TAC. The effects of correction for metabolites and partial volume were investigated. The blood volume fraction in tissue was included in the model and estimated as a fifth parameter. The influx rate constant K was calculated as $k_1 \times k_3 / (k_2 + k_3)$.

In our study, no blood metabolites were measured. The metabolite data of the publications of Visvikis on FLT in colorectal cancer [9] and of Muzi on FLT in lung cancer [10] were extracted. The metabolite data of these two studies appeared similar. They were pooled and fitted with a theoretical curve, as an approximation of metabolite fraction over time. For our experiments we used:

$$\text{Metabolite Fraction} = 0.42 \times (1 - \exp(-0.029 \times T))$$

Partial volume

Another adverse effect in PET imaging is partial volume. We determined the recovery coefficient experimentally using commercially available i.v. tubings to simulate the size of brain vessels. In Fig. 1 the measured recovery coefficient is plotted as a function of tubing diameter for our PET system. The size of the transverse sinuses is estimated at 7–10 mm and a recovery coefficient of 0.7 was chosen to convert the image-based measured blood TAC to the input function. Since the tumors were relatively large (>15 mm), compared with the image resolution, the recovery coefficient of the output function was set to unity.

Statistical analysis

The two-sample rank test (Wilcoxon-Mann-Whitney or Mann-Whitney U test) was used to compare the kinetic parameters obtained under different conditions, and FLT uptake between subgroups. Results are presented as the mean \pm 1 standard deviation. Linear regression analyses

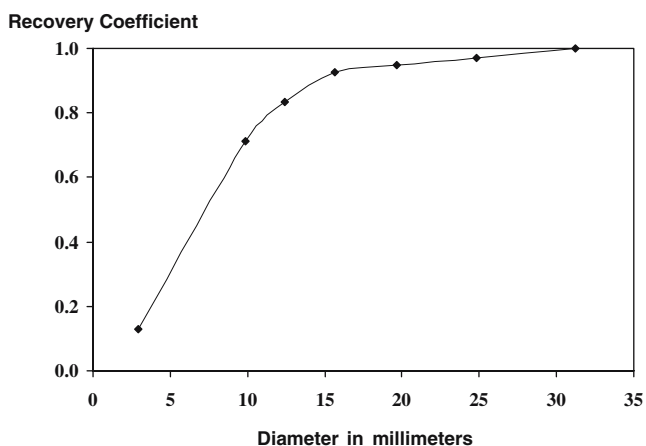


Fig. 1 Recovery coefficient as a function of tubing diameter in millimeters for the ECAT HR+ system

were performed to study the correlation between subgroups, and ANOVA to study differences between patient groups.

Results

Parametric images and time-activity curves

In Fig. 2a, typical slices are shown of the factor image representing vascular structures, e.g., the transverse and cavernous sinuses. The input function was derived from the transverse sinuses by using a 50% threshold to create the VOI and generate a TAC from the dynamic dataset with this VOI. In Fig. 2b, the factor images of a right frontal tumor are shown. Using a 75% threshold to generate the VOI, the tumor TAC was generated, i.e., the output function. The vascular and tumor curves of this patient are shown in Fig. 2c.

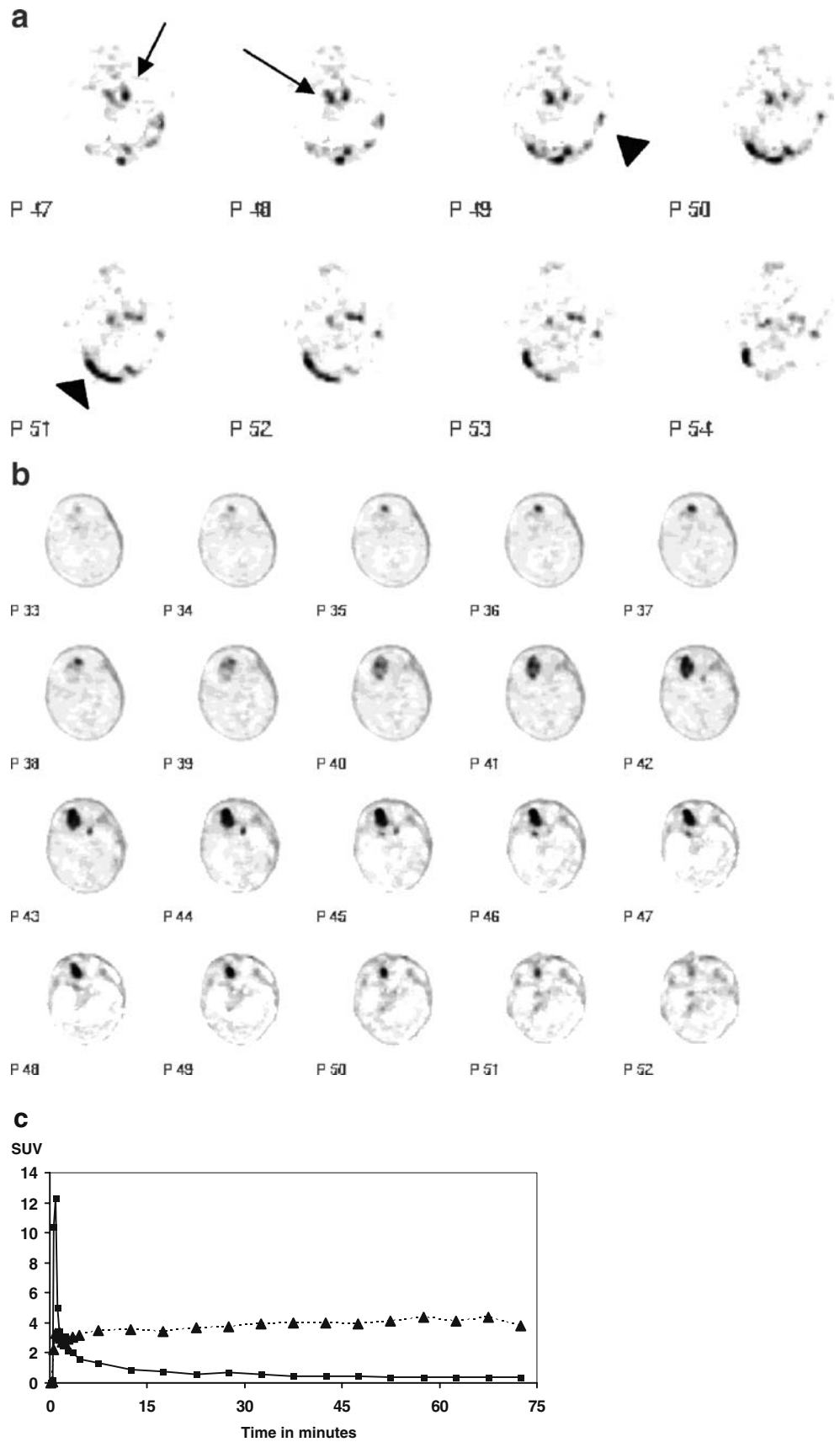
Kinetic modeling

The kinetic parameters for all 18 tumors are given in Table 1, using a three-compartment model with four rate constants and the blood volume in tissue fraction (V_b) as a fifth parameter. Metabolite correction resulted in a better fit of the TACs. As an error estimate, the weighted sum of the square of residuals was used, i.e., (fitted-measured value)² weighted by frame duration. These error estimates showed significant differences with and without metabolite correction ($p < 0.001$). Values for the influx rate constant K were consistently, and for all cases, higher with metabolite correction than without it ($p < 0.001$, sign test). Inspection of the fitted curves and the residuals revealed that correction for metabolites was necessary. Partial volume correction only affects k_1 and, thus, the value of the influx rate constant K .

Patlak graphical analysis, using the frames between 15 and 75 min after injection, furnished a K_{patlak} value that had a high correlation ($r = 0.96$) with the influx rate constant K . The value of K_{patlak} , however, was consistently lower, and significantly different from K ($p < 0.002$), with a mean of 0.013 for K_{patlak} compared with 0.020 for K .

In our population we also measured the standardized uptake value (SUV) of FLT. The uptake level in the upper quartile of tumor voxels (from 75% to 100%) was used to calculate this SUV. Since the FLT uptake often peaks early [5], we calculated an early (from 15–25 min) and late (from 65–75 min) SUV. The average value for $\text{SUV}_{\text{early}}$ was 1.13 and for SUV_{late} , 1.04. Both have a high correlation coefficient to the influx rate constant K , 0.92 and 0.98, respectively. The scatter diagram is shown in Fig. 3 with the lines of the linear regression analysis. Eliminating the high K values of 0.08/min, which may be considered outliers, furnishes a correlation coefficient $r = 0.60$ ($\text{SUV}_{\text{early}}$) and

Fig. 2 Axial images from a 31-year old male who had a newly diagnosed glioblastoma multi-forme located in the right frontal lobe (patient 1 of Table 1). **a** Factor images representing the vascular component. Note the transverse sinuses (*arrowheads*) and cavernous sinuses (*arrows*). **b** Factor images representing the tumor component. **c** TACs from the transverse sinuses (*squares*) and frontal brain tumor (*triangles*). FLT uptake is expressed in SUV (standardized uptake value)



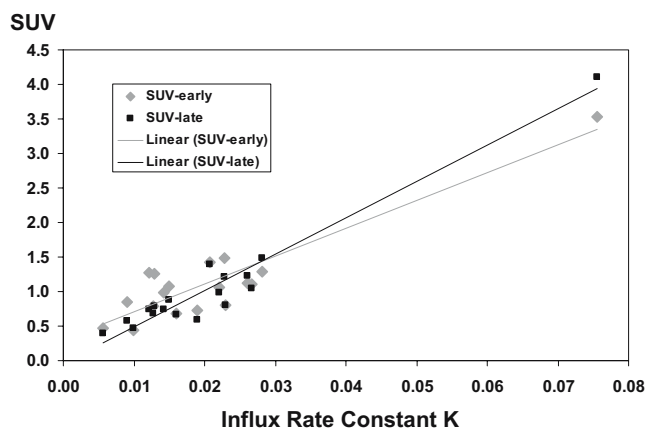


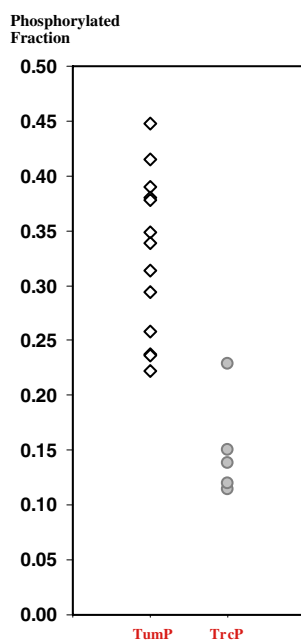
Fig. 3 Scatter diagram of influx rate constant K in min^{-1} vs FLT uptake in SUV. *Gray diamonds* represent the early uptake and *black squares*, the late uptake. The lines are the results of the linear regression analysis, $r=0.92$ (gray) and $r=0.98$ (black). Eliminating the high K values of approx. 0.08 min^{-1} furnished $r=0.60$ (gray) and $r=0.87$ (black), and yielded linear fit slopes that were statistically not different

$r=0.87$ (SUV_{late}), and the slopes of the linear fits of K vs $\text{SUV}_{\text{early}}$ and SUV_{late} were not significantly different.

Comparison of tumor kinetics and biological behavior

Finally, kinetic parameters were correlated with tumor pathology and clinical outcome data. We hypothesized that lesions that consisted predominantly of tumor would have a different kinetic behavior than lesions with predominantly treatment-related changes, i.e., breakdown of the BBB with necrosis and low intracellular metabolism. The time from diagnosis to PET and the outcome in months after PET are given in Table 1. Based on pathology (patients 1 and 4) and

Fig. 4 Plot of the phosphorylated fraction, $k_3/(k_2+k_3)$, for the two patient groups: tumor predominant (*TumP*, diamonds) and treatment change predominant (*TrcP*, circles)



clinical follow-up, two groups could be distinguished: (1) patients with lesions that were tumor predominant (TumP) and (2) patients with lesions that were treatment change predominant (TrcP). The patients in the TumP group had a poorer outcome, with a survival of 1–4 months after the FLT study, except for the two patients with grade III tumors (patients 4 and 5), who are still alive. The patients of the TrcP group had large areas of tumor necrosis on the images and tended to live longer than the patients in the TumP group.

The influx rate constant $K=k_1 \times k_3 / (k_2 + k_3)$ can be rewritten as $k_1 \times f$, with f the fraction of k_1 that ends up in the bound or phosphorylated FLT pool. A plot of this fraction, $k_3 / (k_2 + k_3)$, or the slope between influx rate constant K versus transport k_1 , is shown in Fig. 4. This fraction represents the transported FLT that is ultimately phosphorylated. ANOVA of the regression coefficients over groups revealed highly significant ($p < 0.001$) differences in slopes. Figure 4 shows that the phosphorylated fraction of FLT was higher for the TumP group, with almost no overlap with the TrcP group. The range of transport across the BBB was similar for the two groups, but the influx rate constant was lower for patients with predominantly post-treatment changes (Table 1). This finding is a direct result of the significantly lower phosphorylation rate, k_3 . The mean k_3 was $0.02/\text{min}$ for the TrcP group, compared with $0.11/\text{min}$ for the TumP group. Statistically significant differences between the groups were found for k_3 ($p < 0.01$) but not for k_1 ($p = 0.3$) or K ($p = 0.07$).

All data were processed a second time, i.e., generation of VOIs, TACs, and kinetic modeling, in order to assess variations in the parameter estimates due to the data processing procedure. Table 2 shows the results compared with the standard error of the estimate (SEE) of the parameters. The differences between processing runs were much smaller than the standard error. With some smoothing of the output function, i.e., a 1:2:1 averaging over frames, the effect on the k_1 estimate was the largest (almost comparable to the SEE of k_1), whereas the effect on the other parameters was relatively small.

Table 2 Variations in parameter estimates

Parameter	k_1	k_2	k_3	k_4	V_b
SEE	0.0060	0.0135	0.0053	0.0030	0.0151
Difference	0.0010	0.0029	0.0013	0.0002	0.0022
After smooth	0.0053	0.0051	0.0005	0.0010	0.0024

The *top row* gives the standard error of the estimate (SEE) of each parameter, which is calculated from the covariance matrix obtained during curve fitting. The *middle row* displays the average difference between two processing runs. The *bottom row* shows the average difference in parameter estimates with and without smoothing of the output function (averaging over frames with a 1:2:1 kernel)

Discussion

In this study, the kinetics of FLT in malignant brain tumors were investigated and compared with clinical outcome data. Our analysis is completely image based and virtually operator independent. The factor analysis takes all voxels within the head contour into account. A data-reduction step entails rebinning to voxels of 4.9 mm in x , y , and z dimensions. The factor (parametric) images yield the vessels and tumors, which can be delineated by simple thresholding techniques. The only manual step is to select the structure for processing on the factor image by drawing a large mask around this structure, i.e., the transverse sinus or the tumor. The thresholding algorithm will automatically create the VOI in x , y , and z dimensions within the mask. The VOI comprises all voxels in the 3D volume set that fulfill the criterion. These VOIs are used to generate the TAC of the vascular structure and the tumor.

In earlier work, we have demonstrated that FA can reliably generate an input function. FA-derived input curves were compared with: (1) arterial plasma samples in bone disorders with ^{18}F -fluoride [18], (2) arterialized blood in breast cancer with ^{18}F -FDG [19] and prostate cancer with ^{11}C -acetate [20, 21], and (3) regions drawn over the left ventricular blood pool in myocardial perfusion and metabolism studies with ^{13}N -ammonia and ^{18}F -FDG [22], and myocardial perfusion studies with ^{15}O -water [23]. These studies have shown consistently that kinetic parameters obtained with an FA-based input function are similar to those obtained with a sampled blood curve, and no statistically significant differences were found for the rate constants obtained with these TACs [15, 21].

In this study we used iterative algorithms to reconstruct the images. In earlier work we have shown that the kinetic parameters can be estimated reliably and accurately with these less noisy reconstruction techniques [24, 25]. In many studies, filtered back projection is used as the reconstruction technique. This produces images with high noise levels, especially when the activity is low, as in the current low-dose FLT acquisitions. FA is sensitive to noise, and lower noise levels lead to more accurate derivation of the vascular and tumor factors. The spatial resolution is not constant throughout the image with iterative reconstruction techniques; therefore, a Gaussian smooth was used to make it more uniform.

Corrections for blood volume, metabolites, and partial volume are necessary to produce a good fit between the measured and the model-generated tumor TAC. We did not measure the individual metabolites, as this would have increased the complexity of the study. Instead, we pooled the data of two published studies, which had metabolite curves that looked quite similar. About 2 h after FLT administration, the metabolites comprise 40–42% of the vascular compartment. Our data show that reliable fits can

be obtained with a theoretical metabolite curve. In patients, the metabolites can be accurately fitted with a monoexponential function, as was reported previously [10]. The fact that the metabolite data were similar for lung and colorectal cancer patients led us to believe that they could also be used for brain tumors, which has not yet been confirmed. The effect of metabolites is that the FLT available for transport and phosphorylation is smaller than the actual ^{18}F measured by the PET scanner. On average, metabolite correction causes an increase of approx. 25% in k_3 and K , a decrease of approx. 10% in k_2 , and no change in k_1 and k_4 compared with no metabolite correction. Overestimation of the metabolite fraction leads to a lower value of k_2 and a higher value of k_3 and, thus, to a higher influx rate constant K .

A partial volume correction was applied to the blood curve derived from the images. We did not measure the recovery coefficient for individual patients, but used 0.7 as an estimate of the transverse sinus for our PET system. This limitation can be easily overcome with the latest generation of dual-modality scanners (PET/CT), which allow correction for partial volume effects on an individual basis. Even VOI generation may be simplified, by drawing directly onto the anatomical images. Thus, the FA and vascular TAC generation, which take about half an hour on our current SUN UltraSPARC-60 workstation, might be eliminated. On the other hand, FA will remain important for the generation of the tumor TAC, since it highlights the metabolically active and therefore viable part of the tumor. Parameters derived from this part of the tumor turned out to correlate with the biological behavior of the neoplasm, i.e., predominantly tumor with rapid disease progression versus treated tumor with a decreased phosphorylation rate (k_3). Tumor heterogeneity can be taken into account by including more factors in the FA. More studies are necessary to confirm our observations in larger patient groups.

It is paramount to realize that only the top quartile of voxels is used for analysis, by using a tumor threshold of 75%. Necrotic zones have insufficient FLT uptake and, therefore, do not reach the threshold of 75% uptake of the tumor maximum. The voxels with the top 25% values are selected in order to reduce fluctuations. In this way, we arrive at a less noisy estimate of the FLT uptake than by using the TAC from the voxel with the maximum SUV. Self-evidently, this leads to more reliable fitting and estimation of tumor kinetic parameters. In other words, the lower values in the predominantly post-treatment changes group are not caused by an averaging effect from macroscopic necrosis in the tumor. Areas with macroscopic necrosis are explicitly excluded during the VOI creation step, by ignoring areas of low FLT uptake.

Muzi et al. have shown in their mathematical studies of FLT kinetics that the FLT transport (k_1) can be estimated

with 15% accuracy, whereas FLT influx (K) can be estimated with 5% accuracy [11]. The other parameter estimates are less accurate, even with data acquisition times of 2 h.

The subdivision into groups with lesions that were tumor predominant versus lesions that were treatment change predominant was based on subsequent pathology and clinical follow-up data. These two categories showed different kinetics. The transport across the BBB was quite similar, but the phosphorylation rate, k_3 , and the phosphorylated fraction, $k_3/(k_2+k_3)$, were significantly different ($p<0.001$). The difference in the FLT influx rate constant K did not reach statistical significance ($p=0.07$). These findings are in agreement with the reported studies [2, 11], showing that transport into the cells is fast and primarily determined by perfusion, whereas the phosphorylation reaction, denoted by k_3 , is the rate-limiting step, determining uptake and retention of FLT in somatic tissue [11]. These FLT results are similar to those obtained with ^{11}C -thymidine PET imaging of malignant brain tumors [26].

For all analyses, k_4 turned out to be quite low, and less than 0.03/min for the various conditions. A significant correlation was found between the influx rate constant determined with Patlak graphical analysis and parameter estimation with non-linear regression, i.e., K_{patlak} and K ($r=0.96$), but the absolute value was about 30% different. This difference is in part related to the corrections applied. In our Patlak implementation, no corrections are applied, whereas compartmental modeling uses blood volume, metabolite, and partial volume corrections. Eliminating all these corrections provides an average value of 0.023/min for K and 0.013/min for K_{patlak} . The systematic difference indicates that although k_4 is small, it is not negligible, and Patlak graphical analysis does not yield accurate estimates of the FLT influx rate constant in brain tumors. No statistically significant differences were found between k_4 in the TumP group versus the TrcP group ($p=0.4$). In an attempt to clarify the role of k_4 , the kinetic model with k_4 fixed to zero was tested. This yielded lower values for the kinetic parameters k_1 , k_2 , k_3 , and K , whereas blood volume fraction V_b was not affected. The decreases for k_1 , k_2 , k_3 , and K were all significant ($p<0.001$). For each and every tumor, the influx rate constant K was lower for the $k_4=0$ model than for the standard model. The error was consistently higher for the $k_4=0$ model, with the exception of one tumor. Thus, it appears that k_4 is important, and cannot be neglected. This is in accordance with the findings of Muzi et al. both in their clinical and in their theoretical paper [10, 11].

Inspection of the individual TACs revealed that the neoplasms with predominantly treatment-related changes have a prominent descending branch with increasing time. Evaluation of the early versus the late SUV furnished an average ratio of 1.07 for the TumP group versus 1.40 for

the TrcP group. The difference between the groups was statistically significant ($p=0.01$). In other words, the TumP group had more of a plateau-shaped TAC, whereas the TrcP group had an early peak followed by a clear decline in FLT uptake. For this type of curve the k_4 cannot be ignored and Patlak graphical analysis yields incorrect estimates of the influx rate constant. In their mathematical studies, Muzi et al. reported that a model with three rate constants (setting k_4 to zero) resulted in a loss of accuracy for K . They also concluded that k_4 cannot be neglected [11].

The blood volume term (V_b) with values ranging from 0.03 to 0.31 cannot be ignored. Although the differences were not significant, there was a tendency toward higher values for treatment change-predominant lesions, which might suggest increased edema. This is supported by the larger distribution volume [$V_d=k_1/(k_2+k_3)$] of FLT in the TrcP group ($V_d=0.62$) compared with the TumP group ($V_d=0.43$; $p=0.07$).

Differences between newly diagnosed and recurrent disease need to be investigated further in larger populations. Our study was not focused on changes due to therapy, and the effect of treatment on kinetic parameters needs to be investigated in much larger patient groups. A high correlation coefficient was found between the influx rate constant in min^{-1} and FLT uptake in SUV, at both early (from 15 to 25 min) and late (from 65 to 75 min) time points. This indicates that simple semiquantitative analysis (in SUV) might be sufficient for clinical applications, i.e., monitoring of therapy.

The limitations of this study are the heterogeneity of tumors, resulting in small numbers per subgroup. Despite the small numbers (e.g., only five lesions with predominantly treatment-related changes), robust effects were found for phosphorylation rate, phosphorylated fraction, and early-to-late uptake ratio, that were statistically significant. The main objective of our study was to describe the FLT kinetics in brain tumors, and to test whether a general three-compartment model is adequate. The published model [11] provided excellent fits if corrections were applied for metabolites, blood volume, and partial volume.

The FLT model is an elegant, non-invasive way of evaluating cellular proliferation [2] that is based on the presumption that FLT influx is a representation of thymidine flux or rate of incorporation into DNA [1]. This hypothesis appears valid in glioma cell lines [3] but needs to be confirmed in human gliomas in vivo. Recently, Muzi et al. reported a study in 12 patients on FLT kinetics in brain gliomas. Arterial blood sampling and metabolite measurements were performed, and the same model as described above was used [27]. These investigators found that kinetic modeling yielded robust estimates of FLT transport and influx. They also found a difference between low- and high-grade tumors. Low phosphorylation rates

appeared to limit the applicability for assessing cellular proliferation.

Conclusion

The FLT kinetics were investigated in malignant brain tumors. The standard three-compartment, two-tissue model with corrections for blood volume, metabolites, and partial volume appeared adequate. Factor analysis was applied to provide image-derived blood clearance and tumor uptake curves, which are not user dependent. Two groups could be distinguished based on pathology and clinical follow-up data: (1) lesions that were tumor predominant and (2) lesions that were treatment change predominant. Significantly different values were found for k_3 between these groups. A high correlation was found between FLT uptake in tumor (SUV) and influx rate constant (K), indicating that simple uptake measurements might be sufficient in clinical practice, e.g., for monitoring of therapy.

Acknowledgements This research was supported by DOE grant DE-FC02-02ER63420. The help of James Sayre, PhD with the statistical analyses was greatly appreciated.

References

- Shields AF, Grierson JR, Dohmen BM, Machulla HJ, Stayanoff JC, Lawhorn-Crews JM, et al. Imaging proliferation in vivo with [^{18}F]FLT and positron emission tomography. *Nat Med* 1998;4(11):1334–6.
- Shields AF. PET imaging with ^{18}F -FLT and thymidine analogs: promise and pitfalls. *J Nucl Med* 2003;44(9):1432–4.
- Toyohara J, Waki A, Takamatsu S, Yonekura Y, Magata Y, Fujibayashi Y. Basis of FLT as a cell proliferation marker: comparative uptake studies with [^3H]thymidine and [^3H]arabinothymidine, and cell-analysis in 22 asynchronously growing tumor cell lines. *Nucl Med Biol* 2002;29(3):281–7.
- Seitz U, Wagner M, Neumaier B, Wawra E, Glatting G, Leder G, et al. Evaluation of pyrimidine metabolising enzymes and in vitro uptake of 3'-[^{18}F]fluoro-3'-deoxythymidine ([^{18}F]FLT) in pancreatic cancer cell lines. *Eur J Nucl Med Mol Imaging* 2002;29(9):1174–81.
- Chen W, Cloughesy T, Kamdar N, Satyamurthy N, Bergsneider M, Liao L, et al. Imaging proliferation in brain tumors with ^{18}F -FLT PET: comparison with ^{18}F -FDG. *J Nucl Med* 2005;46(6):945–52.
- Cobben DC, Elsinga PH, Hoekstra HJ, Suurmeijer AJ, Vaalburg W, Maas B, et al. Is ^{18}F -3'-fluoro-3'-deoxy-L-thymidine useful for the staging and restaging of non-small cell lung cancer? *J Nucl Med* 2004;45(10):1677–82.
- Francis DL, Visvikis D, Costa DC, Croasdale I, Arulampalam TH, Luthra SK, et al. Assessment of recurrent colorectal cancer following 5-fluorouracil chemotherapy using both ^{18}F FDG and ^{18}F FLT PET. *Eur J Nucl Med Mol Imaging* 2004;31(6):928.
- Cobben DC, van der Laan BF, Maas B, Vaalburg W, Suurmeijer AJ, Hoekstra HJ, et al. ^{18}F -FLT PET for visualization of laryngeal cancer: comparison with ^{18}F -FDG PET. *J Nucl Med* 2004;45(2):226–31.
- Visvikis D, Francis D, Mulligan R, Costa DC, Croasdale I, Luthra SK, et al. Comparison of methodologies for the in vivo assessment of ^{18}F FLT utilisation in colorectal cancer. *Eur J Nucl Med Mol Imaging* 2004;31(2):169–78.
- Muzi M, Vesselle H, Grierson JR, Mankoff DA, Schmidt RA, Peterson L, et al. Kinetic analysis of 3'-deoxy-3'-fluorothymidine PET studies: validation studies in patients with lung cancer. *J Nucl Med* 2005;46(2):274–82.
- Muzi M, Mankoff DA, Grierson JR, Wells JM, Vesselle H, Krohn KA. Kinetic modeling of 3'-deoxy-3'-fluorothymidine in somatic tumors: mathematical studies. *J Nucl Med* 2005;46(2):371–80.
- Yun M, Oh SJ, Ha HJ, Ryu JS, Moon DH. High radiochemical yield synthesis of 3'-deoxy-3'-[^{18}F]fluorothymidine using (5'-*O*-dimethoxytrityl-2'-deoxy-3'-*O*-nosyl-beta-D-threo pentofuranosyl) thymine and its 3-N-BOC-protected analogue as a labeling precursor. *Nucl Med Biol* 2003;30(2):151–7.
- Nuyts J, Baete K, Beque D, Dupont P. Comparison between MAP and postprocessed ML for image reconstruction in emission tomography when anatomical knowledge is available. *IEEE Trans Med Imaging* 2005;24(5):667–75.
- Nuyts J, Michel C, Dupont P. Maximum-likelihood expectation-maximization reconstruction of sinograms with arbitrary noise distribution using NEC-transformations. *IEEE Trans Med Imaging* 2001;20(5):365–75.
- Schiepers C, Hoh CK, Dahlbom M, Wu HM, Phelps ME. Factor analysis for delineation of organ structures, creation of in- and output functions, and standardization of multicenter kinetic modeling. *Proc SPIE* 1999;3661:1343–50.
- Phelps ME, Huang SC, Hoffman EJ, Selin C, Sokoloff L, Kuhl DE. Tomographic measurement of local cerebral glucose metabolic rate in humans with (F-18)2-fluoro-2-deoxy-D-glucose: validation of method. *Ann Neurol* 1979;6(5):371–88.
- Huang SC, Phelps ME, Hoffman EJ, Sideris K, Selin CJ, Kuhl DE. Noninvasive determination of local cerebral metabolic rate of glucose in man. *Am J Physiol* 1980;238(1):E69–82.
- Schiepers C, Wu HM, Nuyts J, Dahlbom M, Hoh CK, Huang SC, et al. F-18 fluoride PET: Is non-invasive quantitation feasible with factor analysis? *J Nucl Med* 1997;38(5 Suppl):93P.
- Schiepers C, Hoh CK, Dahlbom M, Wu HM, Phelps ME. Reproducibility of input functions obtained with factor analysis in breast cancer. *J Nucl Med* 1998;39(5 Suppl):165P.
- Schiepers C, Hoh CK, Seltzer MA, Phelps ME, Dahlbom M. Factor analysis for quantification of ^{11}C -acetate PET in primary prostate cancer. *J Nucl Med* 2000;41(5 Suppl):100P.
- Schiepers C, Hoh CK, Nuyts J, Wu HM, Phelps ME, Dahlbom M. Factor analysis in prostate cancer: delineation of organ structures and automatic generation of in- and output functions. *IEEE Trans Nucl Sci* 2002;49(5):2338–43.
- Wu HM, Hoh CK, Choi Y, Schelbert HR, Hawkins RA, Phelps ME, et al. Factor analysis for extraction of blood time-activity curves in dynamic FDG-PET studies. *J Nucl Med* 1995;36(9):1714–22.
- Schiepers C, Czernin J, Hoh CK, Nuyts J, Phelps ME, Dahlbom M. Factor analysis for automatic determination of myocardial flow in ^{13}N -ammonia PET studies. *J Nucl Med* 2002;43(5 Suppl):52P.
- Schiepers C, Nuyts J, Wu HM, Verma RC. PET with ^{18}F -fluoride: effects of iterative versus filtered backprojection reconstruction on kinetic modeling. *IEEE Trans Nucl Sci* 1997;44:1591–9.
- Schiepers C, Nuyts J, Wu HM, Dahlbom M, Huang SC, Phelps ME. Influence of iterative reconstruction on parameter estimation with three-compartment kinetic modeling. *J Nucl Med* 1997;38(5 Suppl):102P.
- Wells JM, Mankoff DA, Eary JF, Spence AM, Muzi M, O'Sullivan F, et al. Kinetic analysis of 2-[^{11}C]thymidine PET imaging studies of malignant brain tumors: preliminary patient results. *Mol Imaging* 2002;1(3):145–50.
- Muzi M, Spence AM, O'Sullivan F, Mankoff DA, Wells JM, Grierson JR, et al. Kinetic analysis of 3'-deoxy-3'- ^{18}F -fluorothymidine in patients with gliomas. *J Nucl Med* 2006;47(10):1612–21.